Towing, breathing, splitting, and overtaking in driven colloidal liquid crystals

A. Härtel, R. Blaak, and H. Löwen
Institut für Theoretische Physik II: Weiche Materie, Heinrich-Heine-Universität Düsseldorf, Universitätsstraße 1, D-40225 Düsseldorf, Germany

(Received 23 December 2009; revised manuscript received 15 April 2010; published 6 May 2010)

The nonequilibrium response of a colloidal liquid-crystalline nematic phase to an external aligning field, which rotates in a plane, is explored by dynamical fundamental measure density-functional theory. Depending on the drive frequency, different dynamical states are found, which are characterized by towing and overtaking of the nematic director by the field as well as by breathing and dynamical splitting of the orientational distribution peak. This complex response can be exploited for smart optical switching and mixing devices.

DOI: 10.1103/PhysRevE.81.051703 PACS number(s): 61.30.Gd, 82.70.Dd, 61.20.Gy

The key mechanisms in optical displays and switching devices are governed by the dynamical response of liquid crystals to external aligning fields [1,2]. In particular, it is essential to understand and control the switching dynamics of the nematic director upon a change in the externally imposed alignment field [3]. Liquid crystals can be composed either by anisotropic molecular or colloidal particles with orientational degrees of freedom. The latter have the advantage that they can be studied directly in real space [4–6]. Due to their orientational degrees of freedom, the rheological behavior and nonequilibrium dynamics of rodlike particles are much more complex than that of spherical particles [7]. For instance, for imposed shear flow, the nematic director exhibits an intricate dynamical behavior, which can be classified as tumbling, wagging, kayaking, log rolling, and flow aligning [8–14].

Motivated by the importance of changing alignment fields, we investigate the dynamics of a colloidal nematic phase in the presence of an orientating field, which rotates in a plane with a frequency ω_0. We find a wealth of different dynamical states as a function of system density and external drive frequency. For very small frequencies, the field tows the nematic director such that the latter is rotating with the same external frequency ω_0 in the same plane. During this *towing* process the orientational distribution function keeps a time-independent internal shape. Above a threshold frequency, the width of the orientational distribution exhibits an internal oscillation with another frequency ω_b, an effect that we call orientational *breathing*—in analogy to particles in oscillating traps [15,16]. Further, above a higher threshold frequency, the peak of the orientational distribution splits into two peaks what we refer to as *splitting*. For an even higher external rotation frequency ω_0, the driven nematics cannot follow the drive any longer and is decelerated; rotating with another angular velocity ω_p it is *overtaken* by the external field. Finally, for even higher ω_0, the monopeak is re-entrant before the orientational distribution becomes static in the limit $\omega_0 \to \infty$.

Our studies are based on the microscopic dynamical density-functional theory for Brownian rodlike particles [17] with a recently developed fundamental measure equilibrium density functional [18], which accounts for nontrivial correlations in the inhomogeneous system. This functional is employed for hard spherocylinders in an external time-dependent driving field and has been tested carefully in previous work [19]. Thereby a microscopic approach for nonequilibrium dynamics in dense liquid crystals has been established.

The dynamical states of towing, breathing, splitting, and overtaking, which are predicted by our dynamical density-functional theory, can be confirmed in various systems using different experimental setups. Apart from molecular liquid crystals in rotating aligning fields [20–23], rodlike colloidal particles form nematic phases and can be exposed to rotating electric [24] or magnetic [6,25] aligning fields. A similar effect occurs in ferrofluids in rotating magnetic fields [26] or in complex plasmas of rodlike particles in rotating electric fields [27]. As an equivalent setup, one can rotate the sample and keep the aligning field static, which was proposed recently in Ref. [26]. The different dynamical states in the switching response of the colloidal liquid crystal can be exploited to fabricate smart devices, which generate polarization amplification and mixing.

In our model, we employ hard spherocylinders for lyotropic colloidal liquid crystals in the absence of system boundaries. The spherocylinders have a fixed aspect ratio $L/\sigma=5$,[1] where L is the length of the cylindrical part and σ is the diameter. The averaged number density of the spherocylinders $\bar{\rho}$ is typically chosen in the region where the bulk phases are isotropic or nematic [28]. In the following we express $\bar{\rho}$ in a reduced form via $\rho^\star=\bar{\rho}/\rho_{\mathrm{cp}}$ with the close packing density $\rho_{\mathrm{cp}}\sigma^3=\frac{2}{\sqrt{2}+L/\sigma\sqrt{3}}$. The spherocylinders perform completely overdamped Brownian motion in a solvent, which keeps them at finite temperature T. A time-dependent external driving field is then applied, which brings the suspension into nonequilibrium. The nonequilibrium dynamics are characterized in terms of a time-dependent one-particle density field $\rho(\hat{u},t)=\bar{\rho}f(\hat{u},t)$,[2] which is homogeneous in the translational but heterogeneous in the orientational variable given by an orientational vector $\hat{u}$ on the unit sphere S_2. We remark that although the density field is translational homogeneous the density functional still contains nontrivial positional correlations. In polar coordinates, this unit vector can be expressed by the polar and azimuthal angles, $\hat{u}(\varphi,\vartheta)$

[1]Larger aspect ratios do not change the qualitative dynamical scenario of the dynamical state diagram.

[2]The one-body density is a statistical average over different directors in domains.

TABLE I. Characterization of the different dynamical states via the breathing frequency ω_b, the splitting parameter $\mathcal{N}$, and the averaged angular velocity ω_p of the peak.

	ω_b	$\mathcal{N}$	ω_p
Towing	$=0$	$=1$	$=\omega_0$
Breathing	>0	$=1$	$=\omega_0$
Splitting	>0	$=2$	$=\omega_0$
Overtaking	>0	$=2$	$<\omega_0$
Unsplit and overtaking	>0	$=1$	$<\omega_0$

$=(\cos\varphi\sin\vartheta,\sin\varphi\sin\vartheta,\cos\vartheta)$. The dimensionless and normalized quantity $f(\hat{u},t)$ measures the distribution of orientations of the spherocylinders at a given time t on the unit sphere. Clearly, as we are dealing with apolar particles, $f(-\hat{u},t)=f(\hat{u},t)$.

As for a microscopic theory for nonequilibrium dynamics, we apply dynamical density-functional theory, which provides a deterministic equation for $f(\hat{u},t)$ in a time-dependent external potential. For orientational degrees of freedom, the evolution equation of dynamical density-functional theory in the absence of hydrodynamic interactions is [29]

$$k_BT\bar{\rho}\frac{\partial f(\hat{u},t)}{\partial t}=D_r\hat{R}\cdot\left[f(\hat{u},t)\hat{R}\frac{\delta\mathcal{F}[f]}{\delta f(\hat{u},t)}\right]. \quad (1)$$

Here, D_r is the rotational short-time diffusion constant, which sets the Brownian time scale $\tau_B=1/D_r$ and includes rotational friction, k_BT is the thermal energy, and $\hat{R}=\hat{u}\times\vec{\nabla}_{\hat{u}}$ is the rotational operator. Note that hydrodynamic interactions can be neglected if the physical volume fraction is smaller than the effective volume fraction of the interactions, as realized, e.g., for charged rods. Backflow effects [30] are also not considered. However, it is clear that hydrodynamic interactions between the spherocylinders are important for large physical volume fractions and would lead to more complex dynamical response. Finally all microscopic information is contained in the equilibrium free-energy density functional $\mathcal{F}[f(\hat{u})]$. The latter is conveniently decomposed into three terms $\mathcal{F}[f]=\mathcal{F}_{id}[f]+\mathcal{F}_{ext}[f]+\mathcal{F}_{exc}[f]$, where $\mathcal{F}_{id}[f]=k_BT\int_{S_2}d^2\hat{u}f(\hat{u})[\ln(f(\hat{u}))-1]$ is the entropy of ideal rotators, $\mathcal{F}_{ext}[f]=\int_{S_2}d^2\hat{u}f(\hat{u})V_{ext}(\hat{u},t)$ describes the coupling to an external time-dependent potential $V_{ext}(\hat{u},t)$, and $\mathcal{F}_{exc}[f]$ involves the particle correlations. For the latter we use the recently proposed fundamental measure theory by Hansen-Goos and Mecke [18].[3]

The external aligning potential is chosen as

$$V_{ext}(\hat{u},t)=-V_0\cos^2(\omega_0t-\varphi)\sin^2(\vartheta) \quad (2)$$

and describes a rotation of an optimal alignment direction $\hat{u}_0(t)=\pm(\cos\omega_0t,\sin\omega_0t,0)$ in the equatorial plane of the unit sphere with an external frequency ω_0 and an amplitude $V_0=5k_BT$. The $\pm$ sign reflects the symmetry of apolar particles. This is schematically shown in Fig. 1.

[3]The technical ξ parameter is fixed to 1.6.

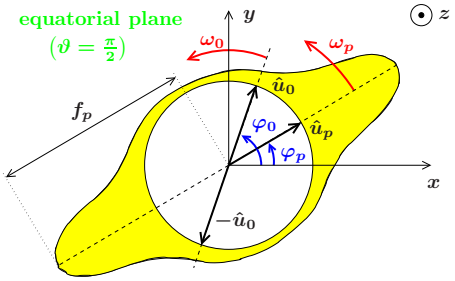

FIG. 1. (Color online) Schematic view of an orientational profile $f(\varphi,\vartheta)$ in the equatorial plane. The surface of the shaded area is given by $f(\varphi,\vartheta)\hat{u}$ with $\hat{u}$, i.e., it is a polar plot of $f(\hat{u})$; f_p is the peak value in the direction $\hat{u}_p$ of the maximum of f. The amplitude of the driving field is maximal along the unit vector $\hat{u}_0$. The external frequency ω_0 and the peak angular velocity ω_p are also indicated.

We have solved the Eq. (1) numerically for $f(\hat{u},t)$ by using a finite difference scheme with a time step of $\Delta t=5\times10^{-5}\tau_B$. Various combinations of reduced densities $\rho^\star$ and external frequencies ω_0 were explored by starting with a homogeneous orientational distribution. After typically 500 cycles, the system reaches a dynamical state, which we characterize by several order parameters. In fact, five qualitative different dynamical orientational distributions are found for increasing frequency. Let us first describe them step-by-step before providing the full nonequilibrium state diagram in the $\rho^\star-\omega_0$ parameter space.

For vanishing ω_0, the external potential is static and leads, at any density $\rho^\star$, to a nematic state with a director along the x axis. For $\omega_0\to\infty$, on the other hand, the system effectively feels a static time-averaged external potential $-V_0\sin^2(\vartheta)/2$. Here the system undergoes a paranematic-nematic transition at about $\rho^\star=0.3717$ [17]. Apart from these two bracketing equilibrium limits, the system shows a complex nonequilibrium response at finite frequencies ω_0. For small ω_0, the external field drags the orientational field $f(\hat{u},t)$ slowly such that its peak position $\hat{u}_p(t)$ follows the optimal orientation $\hat{u}_0(t)$ with the same angular velocity ω_0 and keeps a constant internal shape. We call this dynamical state as towing. The characteristic dynamics in the towing state is summarized in Fig. 2(a). In the left plot, the unit sphere is mapped onto a rectangular stripe showing the height of $f(\hat{u},t)$ for a fixed time. The latter is indicated by an arrow on the time axis of the right plot. The white cross in the left plot indicates the position of $\hat{u}_0(t)$ at this time and reveals the towing behavior.[4] Full time-dependent movies for $f(\hat{u},t)$ are also available [31]. During the towing process, the peak amplitude $f_p(t)=\max_{\varphi,\vartheta}f(\varphi,\vartheta,t)$ is constant and its polar angle $\varphi_p(t)$ is lagging behind the polar angle $\varphi_0(t)$ of $\hat{u}_0(t)$ as given by the solid and dotted lines in the right plot of Fig. 2(a). Obviously, the polar angles are only unique up to a multiple of π, therefore multiple lines are shown in the left plot of Fig. 2(a).

Above a threshold frequency, the peak amplitude $f_p(t)$

[4]The towing behavior is qualitatively similar to the propagating soliton state found in a confined liquid crystal in [C. Zheng and R. B. Meyer, Phys. Rev. E 56, 5553 (1997)].

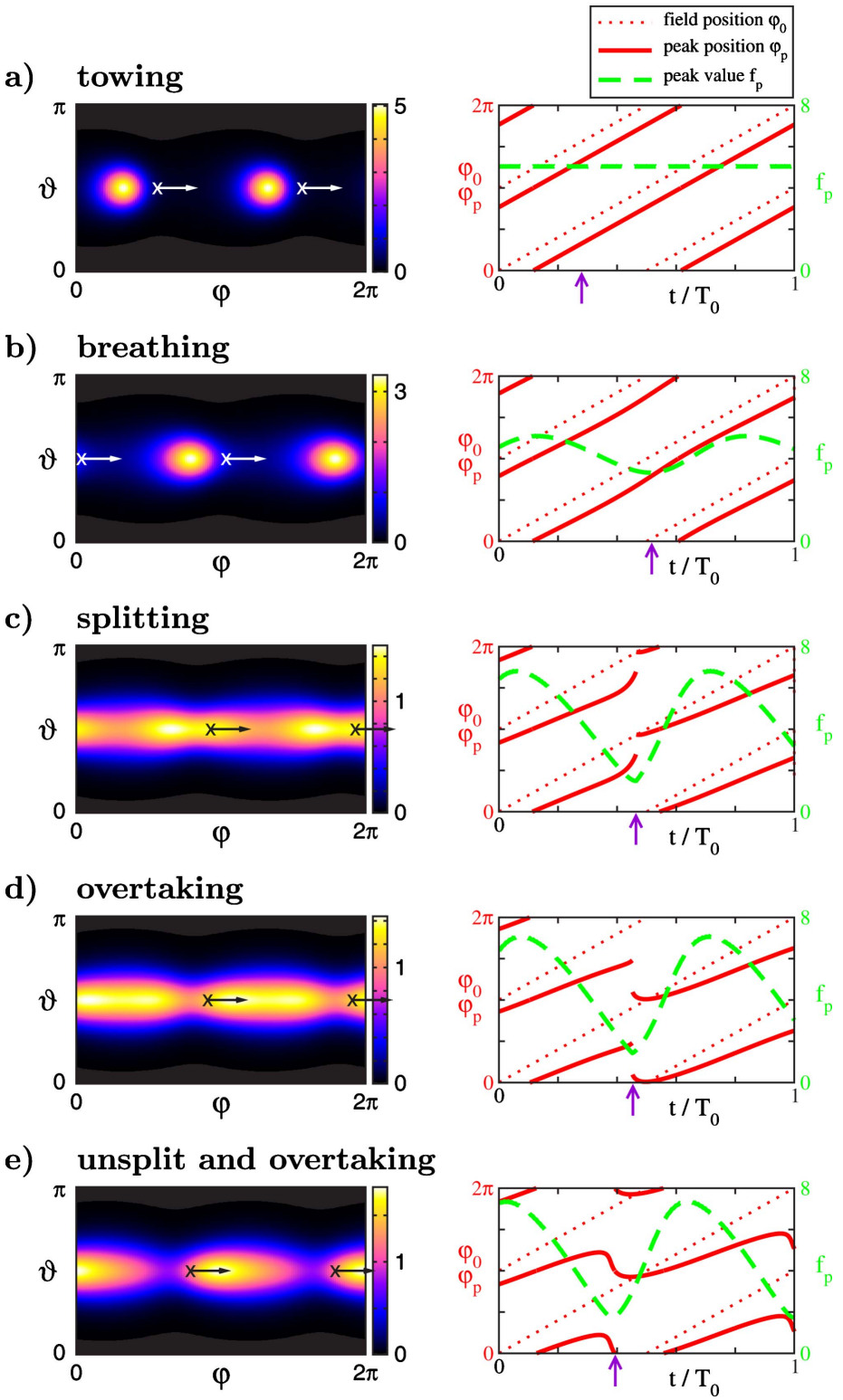

FIG. 2. (Color online) Left figures: orientational distribution function $f(\varphi,\vartheta,t)$ for fixed time given by the arrow on the time axis in the right figure. The cross shows the position of $\hat{u}_0(t)$. Right figures: polar angles of the peak maximum (solid line) and of $\hat{u}_0(t)$ (dotted line) and the peak amplitude f_p (dashed line) versus reduced time t/T_0 along one cycle of the driving potential. The parameters are $\rho^\star=0.5$ and (a) $\omega_0\tau_B/2\pi=0.8$, (b) 0.9, (c) 1.02, (d) 1.07, (e) 1.16.

starts to oscillate with another internal breathing frequency ω_b different from ω_0, see the dashed line in the right plot of Fig. 2(b). The position of the maximum $\varphi_p(t)$ follows the drive position $\varphi_0(t)$ with the same speed on average but has an internal breathing oscillation on top of that, see the solid line in the right plot of Fig. 2(b). The intuitive explanation of the breathing process is that the peak is dragged and pushed periodically by the two bracketing minima of the rotating potential.

If ω_0 is increased further, the peak of $f(\varphi,\vartheta,t)$ splits into two peaks in solid angle (φ,ϑ) space. For this splitting a convenient order parameter is the maximal peak number $\mathcal{N}=\max_t N_{\max}[f(\varphi,\vartheta,t)]$, where $N_{\max}[f(\varphi,\vartheta,t)]$ counts any maxima on a hemisphere (such that $N_{\max}=1$ describes a

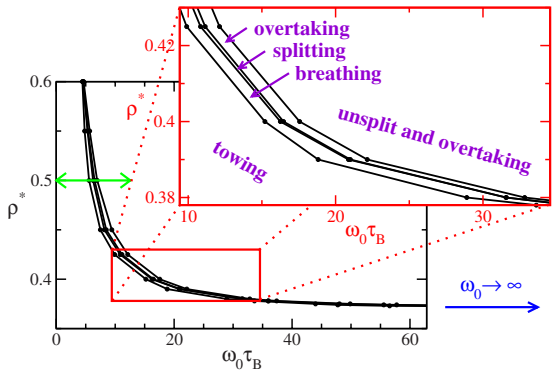

FIG. 3. (Color online) Nonequilibrium state diagram in the plane of driving frequency ω_0 and reduced density $\rho^\star$. The double headed arrow at $\rho^\star=0.5$ is marking the range of $(\omega_0,\rho^\star)$ for that snapshots were taken in Fig. 2. The arrow at the right side gives the position ($\rho^\star\approx 0.3717$) of the static paranematic-nematic transition in the limit $\omega_0\to\infty$.

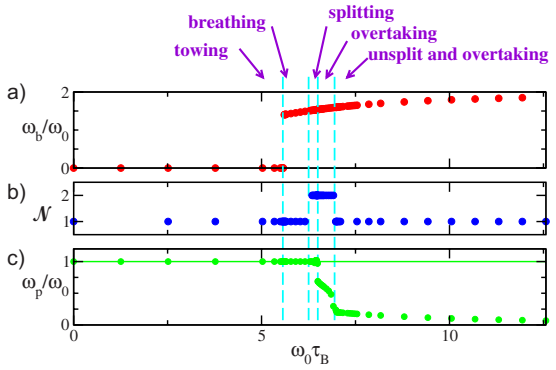

FIG. 4. (Color online) Behavior of (a) the breathing frequency ω_b, (b) the splitting parameter $\mathcal{N}$, and (c) the averaged angular velocity ω_p of the peak shown against the external driving frequency ω_0. The transitions are marked by the vertical slashed lines and the arrows are pointing at those frequencies ω_0 shown in Fig. 2. The density is $\rho^\star=0.5$ (double headed line in Fig. 3).

monopeak and $N_{\max}=2$ a split peak). A splitting state is shown in Fig. 2(c). The function $N_{\max}[f(\varphi,\vartheta,t)]$ is periodic in time with the internal breathing frequency ω_b. Since the angle $\varphi_p(t)$ corresponds to the peak of $f(\varphi,\vartheta,t)$ with maximal amplitude, it jumps during the splitting process [see right plot of Fig. 2(c)], which is associated with a cusp in $f_p(t)$. At higher ω_0, this jump exceeds $\pi/2$. We compose a unique function $\varphi_p(t)$ by coupling branches of $\varphi_p(t)$ together such that their jump is always smaller than $\pi/2$. Using this function, we define a mean angular velocity of the peak maximum by $\omega_p=\frac{1}{T_b}\int_0^{T_b}\dot{\varphi}_p(t)dt$, where $T_b=2\pi/\omega_b$ is the breathing period. Therefore, when the jump exceeded $\pi/2$, the averaged angular velocity of the peak becomes $\omega_p<\omega_0$. We call this state as overtaking since the external field is faster than the orientational peak. A characteristic situation is plotted in Fig. 2(d). Finally, for even higher ω_0, there is a monopeak again, a situation referred to as "unsplit and overtaking." Here, there is no ambiguity in $\varphi_p(t)$ and again $\omega_p<\omega_0$. In this dynamical state there is a simple relation between ω_0, ω_b, and ω_p which comes from the fact that during one cycle of breathing [cf. Fig. 2(e)] the peak position moves from one minimum of the potential backward to the next one. This means a backward angular velocity of $\pi/T_b=\omega_b/2$. Hence, the difference between the angular velocity of the driving potential and the backward velocity of $\omega_b/2$ is then equal to the angular velocity ω_p of the peak, resulting in

$$\omega_0=\frac{1}{2}\omega_b+\omega_p. \tag{3}$$

Relation (3) holds also in the towing state as a special case where $\omega_b=0$.

The different dynamical states are summarized in Table I together with their characterizing order parameters ω_b, $\mathcal{N}$, and ω_p.

A nonequilibrium state diagram is shown in Fig. 3 as a function of external frequency ω_0 and reduced density $\rho^\star$. There is a small density-dependent frequency band in which the cascade of different dynamical states occurs. In fact the splitting phase we only found stable above a critical value of $\rho^\star\approx 0.38$. For large ω_0, the transitions tends to the equilibrium paranematic-nematic transition as shown by the arrow in Fig. 3. In Fig. 4 the three order parameters are shown for a fixed density $\rho^\star=0.5$ (along the double headed line in Fig. 3). While the breathing frequency ω_b jumps discontinuously from the towing to the breathing state it behaves continuously across the following transitions. Conversely the angular velocity ω_p of the peak jumps twice discontinuously across the splitting→overtaking and the overtaking →unsplit transition.

In conclusion, an in-plane aligning field that rotates with an external frequency ω_0 gives rise to a complex dynamical orientational response of a colloidal liquid crystal with five different states characterized by towing, breathing, splitting, overtaking, and unsplit overtaking, as ω_0 increases. We finally mention two applications of the dynamical response: first, in microfluidic devices filled with a nematic liquid crystal [32] localized rotating driving fields can be used as micromixers whose mixing efficiency can be conveniently steered by the external driving frequency, in particular in the regime of the unsplit and overtaking state. Second, if an electromagnetic wave is passing through a rotating nematic liquid crystal [33], its polarization can be amplified and nonlinearly changed by tuning the external drive frequency. The internal breathing state will mix another frequency to the wave coming out and the splitting state will induce further nonlinearities. Therefore the dynamical states can in principle be exploited for the construction of smart switching and mixing devices. Moreover we mention that dynamical states are expected for spherical colloids in traveling colloidal wave fields [34] where the equations of motion are formally similar [35]. It also would be interesting to resolve the spatial dependence of the density field. This is particularly important if system boundaries are included. Finally a comparison to Brownian dynamics computer simulations of hard spherocylinders [36,37] would provide a test for the dynamical theory proposed in this paper.

We thank H. H. Wensink, T. Lubensky, and W. Briels for helpful discussions. This work was supported by the DFG via SPP 1296 and SFB TR6.

[1] J.-H. Kim, M. Yoneya, and H. Yokoyama, Mol. Cryst. Liq. Cryst. **433**, 41 (2005).
[2] J. Hoogboom, T. Rasing, A. E. Rowan, and R. J. M. Nolte, J. Mater. Chem. **16**, 1305 (2006).
[3] R. Berardi, L. Muccioli, and C. Zannoni, J. Chem. Phys. **128**, 024905 (2008).
[4] M. P. Lettinga, Z. Dogic, H. Wang, and J. Vermant, Langmuir **21**, 8048 (2005).
[5] M. P. Lettinga, K. Kang, P. Holmqvist, A. Imhof, D. Derks, and J. K. G. Dhont, Phys. Rev. E **73**, 011412 (2006).
[6] D. van der Beek, P. Davidson, H. H. Wensink, G. J. Vroege, and H. N. W. Lekkerkerker, Phys. Rev. E **77**, 031708 (2008).
[7] E. Bodenschatz, W. Zimmermann, and L. Kramer, J. Phys. (France) **49**, 1875 (1988).
[8] R. G. Larson and H. C. Öttinger, Macromolecules **24**, 6270 (1991).
[9] G. Rienäcker, A. Kröger, and S. Hess, Physica A **315**, 537 (2002).
[10] J. Ding and Y. Yang, Rheol. Acta **33**, 405 (1994).
[11] V. Faraoni, M. Grosso, and S. Crescitelli, J. Rheol. **43**, 829 (1999).
[12] M. Grosso, S. Crescitelli, E. Somma, J. Vermant, P. Moldenaers, and P. L. Maffettone, Phys. Rev. Lett. **90**, 098304 (2003).
[13] Y.-G. Tao, W. K. den Otter, and W. J. Briels, Phys. Rev. Lett. **95**, 237802 (2005).
[14] Y.-G. Tao, W. K. den Otter, and W. J. Briels, J. Chem. Phys. **124**, 204902 (2006).
[15] C. Henning, K. Fujioka, P. Ludwig, A. Piel, A. Melzer, and M. Bonitz, Phys. Rev. Lett. **101**, 045002 (2008).
[16] M. Rex and H. Löwen, Phys. Rev. Lett. **101**, 148302 (2008).
[17] H. H. Wensink and G. J. Vroege, Phys. Rev. E **72**, 031708 (2005).
[18] H. Hansen-Goos and K. Mecke, Phys. Rev. Lett. **102**, 018302 (2009).
[19] A. Härtel and H. Löwen, J. Phys.: Condens. Matter **22**, 104112 (2010).
[20] K. B. Migler and R. B. Meyer, Phys. Rev. Lett. **66**, 1485 (1991).
[21] T. Frisch, S. Rica, P. Coullet, and J. M. Gilli, Phys. Rev. Lett. **72**, 1471 (1994).
[22] S. Nasuno, N. Yoshimo, and S. Kai, Phys. Rev. E **51**, 1598 (1995).
[23] H. R. Kim, Y. W. Lee, S. J. Kim, D. W. Kim, C. J. Yu, B. Lee, and S. D. Lee, Ferroelectrics **312**, 57 (2004).
[24] K. Kang and J. K. G. Dhont, EPL **84**, 14005 (2008).
[25] K. R. MacKenzie and G. McKay, Mol. Cryst. Liq. Cryst. **413**, 197 (2004).
[26] E. Wandersman, E. Dubois, F. Cousin, V. Dupuis, G. Meriguet, R. Perzynski, and A. Cebers, EPL **86**, 10005 (2009).
[27] V. Nosenko, A. V. Ivlev, S. K. Zhdanov, M. Fink, and G. E. Morfill, Phys. Plasmas **16**, 083708 (2009).
[28] P. Bolhuis and D. Frenkel, J. Chem. Phys. **106**, 666 (1997).
[29] M. Rex, H. H. Wensink, and H. Löwen, Phys. Rev. E **76**, 021403 (2007).
[30] D. Svenšek and S. Žumer, Continuum Mech. Thermodyn. **14**, 231 (2002).
[31] See supplementary material at http://link.aps.org/supplemental/10.1103/PhysRevE.81.051703 for movies of the five phases over some cycles of the internal frequency in a dynamical state.
[32] N.-T. Nguyen and Z. Wu, J. Micromech. Microeng. **15**, R1 (2005).
[33] A. E. Miroshnichenko, E. Brasselet, and Y. S. Kivshar, Appl. Phys. Lett. **92**, 253306 (2008).
[34] M. C. Jenkins and S. U. Egelhaaf, J. Phys.: Condens. Matter **20**, 404220 (2008).
[35] M. Rex, H. Löwen, and C. N. Likos, Phys. Rev. E **72**, 021404 (2005).
[36] H. Löwen, Phys. Rev. E **50**, 1232 (1994).
[37] H. Löwen, Phys. Rev. E **59**, 1989 (1999).